Available online at www.sciencedirect.com
SCIENCE DIRECT®
International Journal of Heat and Mass Transfer 47 (2004) 5639–5650
International Journal of HEAT and MASS TRANSFER
www.elsevier.com/locate/ijhmt

Turbulent natural convection in a porous square cavity computed with a macroscopic κ–ε model

Edimilson J. Braga, Marcelo J.S. de Lemos *

Departamento de Energia—IEME, Instituto Tecnológico de Aeronáutica—ITA, 12228-900 São Josédos Campos, SP, Brazil

Received 13 November 2003; received in revised form 14 July 2004
Available online 18 September 2004

Abstract

Detailed numerical computations for laminar and turbulent natural convection within a square cavity filled with a fluid saturated porous medium are presented. Heated vertical walls are maintained at constant but different temperatures, while horizontal surfaces are kept insulated. The macroscopic κ–ε turbulence model with wall function is used to handle turbulent flows in porous media. In this work, the turbulence model is first switched off and the laminar branch of the solution is found when increasing the Rayleigh number, Ra_m. Computations covered the range $10 < Ra_m < 10^6$ and $10^{-7} < Da < 10^{-10}$ and made use of the finite volume method. Subsequently, the turbulence model is included and calculations start at high Ra_m, merging to the laminar branch for a reducing Ra_m and for Ra_m less than a certain critical Rayleigh number, Ra_{cr}. This convergence of results as Ra_m decreases can be seen as a characterization of the laminarization phenomenon. For Ra_m values less than around 10^4, both laminar and turbulent flow solutions merge, indicating that such critical value for Ra_m was reached. Results further indicate that when the parameters porosity, Pr, conductivity ratio between the fluid and the solid matrix and the Ra_m are kept fixed, the lower the Darcy number, the higher the average Nusselt number at the hot wall.

Keywords: Turbulence modeling; Porous media; Heat transfer; Natural convection

1. Introduction

Thermal convection in porous media has been studied extensively in recent years. Underground spread of pollutants, grain storage, optimal design of furnaces and solar collectors, crystal growth in liquids, nuclear reactor safety and insulation, as well as food processing, are just some applications of this theme. Further, the analysis of buoyancy-driven flows in clear or porous cavities provides useful comparisons for evaluating the robustness and performance of numerical methods dealing with viscous flow calculations. The modeling of macroscopic transport for incompressible flows in porous media has been based on the volume-average methodology for either heat [1] or mass transfer [2–4]. If the flow fluctuates in time and has in addition to presenting spatial deviations, there are two possible methodologies to follow in order to obtain macroscopic equations: (a) application of time-average operator followed by volume-averaging [5–8], or (b) use of volume-averaging before applying time smoothing [9–11]. It has been shown that both sets of macroscopic mass transport equations are equivalent when examined under the recently established *double decomposition* concept [12–16]. This

* Corresponding author. Tel.: +55 12 3947 5860; fax: +55 12 3947 5842.
E-mail address: delemos@mec.ita.br (M.J.S. de Lemos).

0017-9310/$ - see front matter © 2004 Elsevier Ltd. All rights reserved.
doi:10.1016/j.ijheatmasstransfer.2004.07.017

Nomenclature

c_F	Forchheimer coefficient
$c's$	non-dimensional turbulence model constants
c_p	specific heat
d	pore diameter
$\mathbf{D}$	$\boldsymbol{D} = [\nabla \boldsymbol{u} + (\nabla \boldsymbol{u})^{\mathrm{T}}]/2$, deformation rate tensor
Da	Darcy number, $Da = \frac{K}{H^2}$
D_p	$D_p = \sqrt{\frac{144K(1-\phi)^2}{\phi^3}}$, particle diameter
$\mathbf{g}$	gravity acceleration vector
G_k	buoyancy production rate of turbulent kinetic energy
G^i	generation rate of $\langle k \rangle^i$ due to the action of the porous matrix
G^i_β	generation rate of $\langle k \rangle^i$ due to the buoyant effects
h	heat transfer coefficient
H	square height
$\mathbf{I}$	unit tensor
K	permeability
k	$k = \overline{\mathbf{u}' \cdot \mathbf{u}'}/2$, turbulent kinetic energy per mass unit
k_f	fluid thermal conductivity
k_s	solid thermal conductivity
$\mathbf{K}_{disp}$	conductivity tensor due to the dispersion
$\mathbf{K}_{disp,t}$	conductivity tensor due to the turbulent dispersion
$\mathbf{K}_t$	conductivity tensor due to the turbulent heat flux
$\mathbf{K}_{tor}$	conductivity tensor due to the tortuosity
L	square width
Nu	$Nu = hL/k_{eff}$, Nusselt number
Pe	Peclet number
Pe_D	modified Peclet number, $Pe_D = Pe(1-\phi)^{1/2}$
P_k	shear production rate of turbulent kinetic energy
P^i	production rate of $\langle k \rangle^i$ due to gradients of $\bar{\mathbf{u}}_D$
Pr	Prandtl number
Ra_f	$Ra_f = \frac{g\beta H^3 \Delta T}{\nu_f \alpha_f}$, fluid Rayleigh number
Ra_m	$Ra_m = Ra_f \cdot Da = \frac{g\beta_\phi H \Delta TK}{\nu_f \alpha_{eff}}$, Darcy–Rayleigh number
Ra_{cr}	critical Rayleigh number
Re_p	$Re_p = \frac{\lvert \mathbf{u}_D \rvert d}{\nu_f}$, Reynolds number based on the pore diameter
T	temperature
$\boldsymbol{u}$	microscopic velocity
$\boldsymbol{u}_D$	Darcy or superficial velocity (volume average of $\mathbf{u}$)

Greek symbols

α	thermal diffusivity
β	thermal expansion coefficient
ΔV	representative elementary volume
ΔV_f	fluid volume inside ΔV
ε	$\varepsilon = \mu \nabla \mathbf{u}' : (\nabla \mathbf{u}')^{\mathrm{T}}/\rho$, dissipation rate of k
μ	dynamic viscosity
μ_t	microscopic turbulent viscosity
μ_{t_ϕ}	macroscopic turbulent viscosity
ν	kinematic viscosity
ρ	density
$\sigma's$	non-dimensional constants
ϕ	$\phi = \Delta V_f/\Delta V$, porosity

Special symbols

φ	general variable
$\bar{\varphi}$	time average
φ'	time fluctuation
$\langle \varphi \rangle^i$	intrinsic average
$\langle \varphi \rangle^v$	volume average
${}^i\varphi$	spatial deviation
$\lvert \varphi \rvert$	absolute value (Abs)
$\boldsymbol{\varphi}$	general vector variable
φ_{eff}	effective value, $\varphi_{eff} = \phi\varphi_f + (1-\phi)\varphi_s$
$\varphi_{s,f}$	solid/fluid
$(\varphi)_{H,C}$	hot/cold
$(\varphi)_\phi$	macroscopic value
$()^{\mathrm{T}}$	transpose

methodology has been extended to heat transfer in porous media where both time fluctuations and spatial deviations were considered for velocity and temperature [17,18]. Studies on the treatment of interface conditions [19,20], on buoyant flows [21], mass transfer [22] and double diffusion [23], in addition to a general classification of models [24], have also been published.

Natural convection occurs in enclosures as a result of gradients in density which, in turn, is due to variations in temperature or mass concentration. Natural convection in an infinite horizontal layer of fluid, heated from below, has received extensive attention since the beginning of the 20th century when Bérnard [25] observed hexagonal roll cells upon the onset of convection in molten spermaceti with a free upper surface. The work of Rayleigh [26] was the first to compute a critical value, Ra_c, for the onset of convection. The accepted theoretical value of this dimensionless group is 1708 for infinite rigid upper and lower surfaces. The study of natural convection in enclosures still attracts the attention of researchers and a significant number of experimental and theoretical works have been carried out mainly from the 80s.

During the conference on Numerical Methods in Thermal Problems, which took place in Swansea, [27] proposed that buoyancy-driven flow in a square cavity would be a suitable vehicle for testing and validating computer codes. Following discussions at Swansea, contributions for the solution of the problem were invited. A total of 37 contributions from 30 groups in nine different countries were received. The compilation and discussion of the main contributions yielded the classical benchmark of [28].

The first to introduce a turbulence model in their calculations were [29]. They performed steady 2-D simulations for Ra up to 10^{16} and presented a complete set of results. Ref. [30] used the same turbulence model adopted by them for 2-D calculations up to $Ra = 10^{11}$.

In [31], 2-D calculations using various versions of the κ–ε turbulence model were performed. These versions included the standard as well as the low-Reynolds number κ–ε models.

In [32], 3-D calculations for laminar flow for Ra up to 10^{10} were presented. Their graphs revealed the 3-D character of the flow. Comparisons were made with 2-D simulations and differences were reported for the heat transfer correlation between Nu and Ra.

The paper of [33] reworked the problem for laminar and turbulent flows for a wide range of Ra. Turbulence was modeled with the standard κ–ε closure and the effect of the assumed wall functions on heat transfer was investigated.

The monographs of [34] and [35] fully document natural convection in porous media.

The case of free convection in a rectangular cavity heated on a side and cooled at the opposing side is an important problem in thermal convection in porous media. The works of [36–42] have contributed with some important results to this problem.

The recent work of [43], concerned a numerical study of the steady free convection flow in rectangular and oblique cavities filled with homogeneous porous media using a nonlinear axis transformation. The Darcy momentum and energy equations are solved numerically using the (ADI) method.

Motivated by the foregoing work, this paper presents results for both laminar and turbulent flows in a square cavity totally filled with a porous material, heated from the left and cooled from the opposing side. The other two walls are kept insulated. The turbulence model here adopted is the macroscopic κ–ε with wall function.

2. The problem under consideration

The problem considered is showed schematically in Fig. 1(a) and refers to a square cavity with side $L = 1$ m completely filled with porous medium. The cavity is isothermally heated from the left, T_H, and cooled from the opposing side, T_C. The other two walls are insulated. These boundary conditions are widely applied when solving buoyancy-driven cavity flows [25]. The porous medium is considered to be rigid and saturated by an incompressible fluid. The Ra_m is the dimensionless parameter used for porous media and it is defined as, $Ra_m = Ra_f Da$, with $\alpha_{eff} = k_{eff}/(\rho c_p)_f$ and the particle diameter is given by $D_p = \sqrt{\frac{144K(1-\phi)^2}{\phi^3}}$.

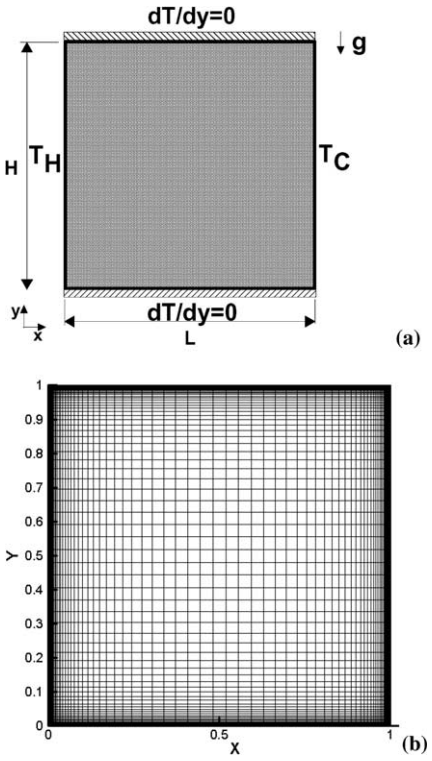

Fig. 1. (a) Geometry under consideration, (b) computational grid.

3. Governing equations

The equations used herein are derived in details in Refs. [12–16] and for this reason their derivation need not be repeated here. It is interesting to point out that the value of porosity, ϕ, in the governing equations to be shown below, is located inside the spatial operator (gradient). As such, no assumption is made on the constancy of ϕ over the domain of calculation. Pedras and de Lemos [13] points out that the only restriction to apply is the constancy of ϕ with time, otherwise, volume and time average operators do not commute.

Basically, for porous media analysis, a macroscopic form of the time-averaged equations is obtained by taking the volumetric mean of the entire equation set

[12–16]. In that development, the medium was considered rigid and saturated by an incompressible fluid. Accordingly, for a general fluid property φ the intrinsic and volumetric averages are related through the porosity ϕ as,

$$\langle\varphi\rangle^{\mathrm{i}} = \frac{1}{\Delta V_{\mathrm{f}}}\int_{\Delta V_{\mathrm{f}}} \varphi \,\mathrm{d}V; \quad \langle\varphi\rangle^{\mathrm{v}} = \phi\langle\varphi\rangle^{\mathrm{i}}; \quad \phi = \frac{\Delta V_{\mathrm{f}}}{\Delta V} \tag{1}$$

where ΔV_{f} is the volume of the fluid contained in ΔV, the volume of a representative elementary volume. The property φ can then be defined as the sum of $\langle\varphi\rangle^{\mathrm{i}}$ and a term related to its spatial variation within the REV, ${}^{\mathrm{i}}\varphi$, as [3],

$$\varphi = \langle\varphi\rangle^{\mathrm{i}} + {}^{\mathrm{i}}\varphi \tag{2}$$

The macroscopic continuity equation is then given by,

$$\nabla\cdot\bar{\mathbf{u}}_{\mathrm{D}} = 0 \tag{3}$$

where the Dupuit–Forchheimer relationship, $\bar{\mathbf{u}}_{\mathrm{D}} = \phi\langle\bar{\mathbf{u}}\rangle^{\mathrm{i}}$, has been used and $\langle\bar{\mathbf{u}}\rangle^{\mathrm{i}}$ identifies the intrinsic (liquid) average of the local velocity vector $\bar{\mathbf{u}}$. The macroscopic time-mean Navier–Stokes (NS) equation for an incompressible fluid with constant properties is given as,

$$\begin{aligned}\rho\left[\frac{\partial\bar{\mathbf{u}}_{\mathrm{D}}}{\partial t} + \nabla\cdot\left(\frac{\bar{\mathbf{u}}_{\mathrm{D}}\bar{\mathbf{u}}_{\mathrm{D}}}{\phi}\right)\right] &= -\nabla\left(\phi\langle\bar{p}\rangle^{\mathrm{i}}\right) + \mu\nabla^2\bar{\mathbf{u}}_{\mathrm{D}} + \nabla\cdot\left(-\rho\phi\langle\overline{\mathbf{u}'\mathbf{u}'}\rangle^{\mathrm{i}}\right)\\ &\quad - \rho\beta_{\phi}\mathbf{g}\phi\left(\langle\overline{T}\rangle^{\mathrm{i}} - T_{\mathrm{ref}}\right) - \left[\frac{\mu\phi}{K}\bar{\mathbf{u}}_{\mathrm{D}} + \frac{c_{\mathrm{F}}\phi\rho|\bar{\mathbf{u}}_{\mathrm{D}}|\bar{\mathbf{u}}_{\mathrm{D}}}{\sqrt{K}}\right]\end{aligned} \tag{4}$$

Before proceeding, a word about the dispersion mechanism seems timely. Bear [2] and Hsu and Cheng [1] have defined, among others, the dispersion mechanism for momentum and heat transport, respectively. Mathematically speaking, dispersion is a space correlation between deviation of a generic flow property and velocity deviation (see Pedras and de Lemos, [12]). When the flow property is velocity, temperature, or mass concentration, one has *mechanical*, *thermal* or *mass* dispersion, respectively. Such mechanism is also present in laminar flow through porous media (low $Re_{\mathrm{p}} = |\boldsymbol{u}_{\mathrm{D}}|d/\nu_{\mathrm{f}}$). Having defined an appropriate nomenclature, considerations about characteristics of the models here employed can be made.

In view of the above, it is interesting to point out that mechanical dispersion has been neglected in Eq. (4). The reason for assuming such hypothesis is based on the fact that this work in intended to model flows in highly permeable, high porosity media, for which the range of pore Reynolds number considered is given by $Re_{\mathrm{p}} > 300$. As such, turbulent flow is assumed to exist within the medium and, under this condition, turbulent transfer (third term on the right of (4)) overwhelms mechanical dispersion (see [13]). For laminar flow with low Re_{p}, however, the greater importance of mechanical dispersion as an effective mechanism of momentum exchange is commonly accepted in the literature. On should point out though that *thermal* dispersion is here not neglected, as will be seen below.

Further, when treating turbulence with statistical tools, the correlation $-\rho\overline{\mathbf{u}'\mathbf{u}'}$ appears after application of the time-average operator to the local instantaneous NS equation. Applying further the volume-average procedure to this correlation results in the term $-\rho\phi\langle\overline{\mathbf{u}'\mathbf{u}'}\rangle^{\mathrm{i}}$. This term is here recalled the *macroscopic Reynolds stress tensor* (MRST). Further, a model for the (MRST) in analogy with the Boussinesq concept for clear fluid can be written as

$$-\rho\phi\langle\overline{\mathbf{u}'\mathbf{u}'}\rangle^{\mathrm{i}} = \mu_{\mathrm{t}_{\phi}} 2\langle\overline{\mathbf{D}}\rangle^{\mathrm{v}} - \frac{2}{3}\phi\rho\langle k\rangle^{\mathrm{i}}\mathbf{I} \tag{5}$$

where

$$\langle\overline{\mathbf{D}}\rangle^{\mathrm{v}} = \frac{1}{2}\left[\nabla(\phi\langle\bar{\mathbf{u}}\rangle^{\mathrm{i}}) + [\nabla(\phi\langle\bar{\mathbf{u}}\rangle^{\mathrm{i}})]^{\mathrm{T}}\right] \tag{6}$$

is the macroscopic deformation rate tensor, $\langle k\rangle^{\mathrm{i}}$ is the intrinsic average for k and $\mu_{\mathrm{t}_{\phi}}$ is the macroscopic turbulent viscosity. The macroscopic turbulent viscosity, $\mu_{\mathrm{t}_{\phi}}$, is modeled similarly to the case of clear fluid flow and a proposal for it was presented in [13] as,

$$\mu_{\mathrm{t}_{\phi}} = \rho c_{\mu}\frac{\langle k\rangle^{\mathrm{i}^2}}{\langle\varepsilon\rangle^{\mathrm{i}}} \tag{7}$$

In a similar way, applying both time and volumetric average to the microscopic energy equation, for either the fluid or the porous matrix, two equations arise. Assuming further the *local thermal equilibrium hypothesis,* which considers $\langle\overline{T}_{\mathrm{f}}\rangle^{\mathrm{i}} = \langle\overline{T}_{\mathrm{s}}\rangle^{\mathrm{i}} = \langle\overline{T}\rangle^{\mathrm{i}}$, and adding up these two equations, one has,

$$\begin{aligned}(\rho c_{\mathrm{p}})_{\mathrm{f}}\nabla\cdot\left(\phi\langle\overline{\mathbf{u}T_{\mathrm{f}}}\rangle^{\mathrm{i}}\right) = (\rho c_{\mathrm{p}})_{\mathrm{f}}\nabla\cdot\Big\{\phi\Big(&\langle\bar{\mathbf{u}}\rangle^{\mathrm{i}}\langle\overline{T}_{\mathrm{f}}\rangle^{\mathrm{i}} + \overline{\langle\mathbf{u}'\rangle^{\mathrm{i}}\langle T'_{\mathrm{f}}\rangle^{\mathrm{i}}}\\ &+\langle{}^{\mathrm{i}}\bar{\mathbf{u}}^{\mathrm{i}}\overline{T}_{\mathrm{f}}\rangle^{\mathrm{i}} + \overline{\langle{}^{\mathrm{i}}\mathbf{u}'^{\mathrm{i}}T'_{\mathrm{f}}\rangle^{\mathrm{i}}}\Big)\Big\}\end{aligned} \tag{8}$$

A modeled form of (8) has been given in detail in the work of [18] as,

$$\begin{aligned}\left\{(\rho c_{\mathrm{p}})_{\mathrm{f}}\phi + (\rho c_{\mathrm{p}})_{\mathrm{s}}(1-\phi)\right\}\frac{\partial\langle\overline{T}\rangle^{\mathrm{i}}}{\partial t} + (\rho c_{\mathrm{p}})_{\mathrm{f}}\nabla\cdot\left(\bar{\mathbf{u}}_{\mathrm{D}}\langle\overline{T}\rangle^{\mathrm{i}}\right)\\ = \nabla\cdot\left\{\mathbf{K}_{\mathrm{eff}}\cdot\nabla\langle\overline{T}\rangle^{\mathrm{i}}\right\}\end{aligned} \tag{9}$$

where, $\mathbf{K}_{\mathrm{eff}}$, given by

$$\mathbf{K}_{\mathrm{eff}} = [\phi k_{\mathrm{f}} + (1-\phi)k_{\mathrm{s}}]\mathbf{I} + \mathbf{K}_{\mathrm{tor}} + \mathbf{K}_{\mathrm{t}} + \mathbf{K}_{\mathrm{disp}} + \mathbf{K}_{\mathrm{disp,t}} \tag{10}$$

is the effective conductivity tensor. In order to be able to apply (9), it is necessary to determine the conductivity tensors in (10), i.e. $\mathbf{K}_{\mathrm{tor}}$, $\mathbf{K}_{\mathrm{t}}$, $\mathbf{K}_{\mathrm{disp}}$ and $\mathbf{K}_{\mathrm{disp,t}}$. Following [7], this can be accomplished for the tortuosity and thermal dispersion conductivity tensors, $\mathbf{K}_{\mathrm{tor}}$ and $\mathbf{K}_{\mathrm{disp}}$, by making use of a unit cell subjected to periodic boundary conditions for the flow and a linear temperature gradient imposed over the domain. The conductivity tensors are

then obtained directly from the microscopic results for the unit cell.

As mentioned earlier, here, *thermal* dispersion is not neglected. Kuwahara and Nakayama [7] presented, for an infinite medium formed by an array of square rods, the $\mathbf{K}_{\text{disp}}$ components in the longitudinal and transversal directions, $(K_{\text{disp}})_{XX}$ and $(K_{\text{disp}})_{YY}$, respectively. Their expressions read,

$$(K_{\text{disp}})_{XX} = \begin{cases} 0.022\frac{Pe_{\text{D}}^2}{(1-\phi)}k_{\text{f}}, & Pe_{\text{D}} < 10 \\ 2.7\frac{Pe_{\text{D}}}{\phi^{1/2}}k_{\text{f}}, & Pe_{\text{D}} > 10 \end{cases}$$
$$(K_{\text{disp}})_{YY} = \begin{cases} 0.022\frac{Pe_{\text{D}}^{1.7}}{(1-\phi)^{1/4}}k_{\text{f}}, & Pe_{\text{D}} < 10 \\ 0.052(1-\phi)^{1/2}Pe_{\text{D}}k_{\text{f}}, & Pe_{\text{D}} > 10 \end{cases} \quad (11)$$

where

$$Pe_{\text{D}} = Pe(1-\phi)^{1/2}; \quad Pe = Re_{\text{p}}\,\text{Pr}; \quad Re_{\text{p}} = \frac{|\mathbf{u}_{\text{D}}|d}{\nu_{\text{f}}} \quad (12)$$

and d is the pore diameter.

The turbulent heat flux and turbulent thermal dispersion terms, $\mathbf{K}_{\text{t}}$ and $\mathbf{K}_{\text{disp,t}}$, which cannot be determined from such a microscopic calculation, are modeled here through the Eddy diffusivity concept, similarly to [8]. It should be noticed that these terms arise only if the flow is turbulent, whereas the tortuosity and the thermal dispersion terms exist for both laminar and turbulent flow regimes.

Starting out from the time averaged energy equation coupled with the microscopic modeling for the 'turbulent thermal stress tensor' through the Eddy diffusivity concept, one can write, after volume averaging,

$$-(\rho c_{\text{p}})_{\text{f}}\langle\overline{\mathbf{u}'T'_{\text{f}}}\rangle^{\text{i}} = (\rho c_{\text{p}})_{\text{f}}\frac{\nu_{\text{t}_\phi}}{\sigma_{\text{T}}}\nabla\langle\overline{T}_{\text{f}}\rangle^{\text{i}} \quad (13)$$

where the symbol ν_{t_ϕ} expresses the macroscopic Eddy viscosity, $\mu_{\text{t}_\phi} = \rho_{\text{f}}\nu_{\text{t}_\phi}$, given by (7) and σ_{T} is a constant. According to (13), the macroscopic heat flux due to turbulence is taken as the sum of the turbulent heat flux and the turbulent thermal dispersion found by [18]. In view of the arguments given above, the turbulent heat flux and turbulent thermal dispersion components of the conductivity tensor, $\mathbf{K}_{\text{t}}$ and $\mathbf{K}_{\text{disp,t}}$, respectively, are expressed as

$$\mathbf{K}_{\text{t}} + \mathbf{K}_{\text{disp,t}} = \phi(\rho c_{\text{p}})_{\text{f}}\frac{\nu_{\text{t}_\phi}}{\sigma_{\text{T}}}\mathbf{I} \quad (14)$$

In the equation set shown above, when the variable $\phi = 1$, the domain is considered as a clear medium. For any other value of ϕ, the domain is treated as a porous medium.

4. Turbulence model

Transport equations for $\langle k\rangle^{\text{i}} = \langle\overline{\mathbf{u}'\cdot\mathbf{u}'}\rangle^{\text{i}}/2$ and $\langle\varepsilon\rangle^{\text{i}} = \mu\langle\overline{\nabla\mathbf{u}':(\nabla\mathbf{u}')^{\text{T}}}\rangle^{\text{i}}/\rho$ in their so-called high Reynolds number form are fully documented in Pedras and de Lemos [12–16] making use of the *double decomposition* concept and extended in de Lemos and Braga [21] to incorporate buoyancy effects. Basically, for porous media analysis, a macroscopic form of the governing equations is here obtained by taking the volumetric average of the time averaged equations set.

As explained in [12], different paths in obtaining a k-equation have been proposed. Lee and Howell [9] and Antohe and Lage [10] developed a macroscopic equation for the turbulent kinetic energy formed as $k_{\text{m}} = \overline{\langle\mathbf{u}'\rangle^{\text{i}}\cdot\langle\mathbf{u}'\rangle^{\text{i}}}/2$. De Lemos and co-workers [12–24] based their model on $\langle k\rangle^{\text{i}} = \langle\overline{\mathbf{u}'\cdot\mathbf{u}'}\rangle^{\text{i}}/2$. The relationship between these two quantities is [12]

$$\langle k\rangle^{\text{i}} = \langle\overline{\mathbf{u}'\cdot\mathbf{u}'}\rangle^{\text{i}}/2 = \overline{\langle\mathbf{u}'\rangle^{\text{i}}\cdot\langle\mathbf{u}'\rangle^{\text{i}}}/2 + \overline{\langle{}^{\text{i}}\mathbf{u}'\cdot{}^{\text{i}}\mathbf{u}'\rangle}/2$$
$$= k_{\text{m}} + \overline{\langle{}^{\text{i}}\mathbf{u}'\cdot{}^{\text{i}}\mathbf{u}'\rangle}/2 \quad (15)$$

For that reason, transport equations for $k_{\text{m}} = \overline{\langle\mathbf{u}'\rangle^{\text{i}}\cdot\langle\mathbf{u}'\rangle^{\text{i}}}/2$ and $\langle k\rangle^{\text{i}} = \langle\overline{\mathbf{u}'\cdot\mathbf{u}'}\rangle^{\text{i}}/2$ are not equal because, as seen, they represent two different quantities being transported [12]. In this work, macroscopic turbulent transport equations are given by [21]

$$\rho\left[\frac{\partial}{\partial t}\left(\phi\langle k\rangle^{\text{i}}\right) + \nabla\cdot\left(\bar{\mathbf{u}}_{\text{D}}\langle k\rangle^{\text{i}}\right)\right] = \nabla\cdot\left[\left(\mu + \frac{\mu_{\text{t}_\phi}}{\sigma_{\text{k}}}\right)\nabla\left(\phi\langle k\rangle^{\text{i}}\right)\right] + P^{\text{i}} + G^{\text{i}} + G^{\text{i}}_{\beta} - \rho\phi\langle\varepsilon\rangle^{\text{i}} \quad (16)$$

$$\rho\left[\frac{\partial}{\partial t}\left(\phi\langle\varepsilon\rangle^{\text{i}}\right) + \nabla\cdot\left(\bar{\mathbf{u}}_{\text{D}}\langle\varepsilon\rangle^{\text{i}}\right)\right] = \nabla\cdot\left[\left(\mu + \frac{\mu_{\text{t}_\phi}}{\sigma_{\varepsilon}}\right)\nabla\left(\phi\langle\varepsilon\rangle^{\text{i}}\right)\right] + c_1P^{\text{i}}\frac{\langle\varepsilon\rangle^{\text{i}}}{\langle k\rangle^{\text{i}}} + c_2\frac{\langle\varepsilon\rangle^{\text{i}}}{\langle k\rangle^{\text{i}}}G^{\text{i}} + c_1c_3G^{\text{i}}_{\beta}\frac{\langle\varepsilon\rangle^{\text{i}}}{\langle k\rangle^{\text{i}}} - c_2\rho\phi\frac{\langle\varepsilon\rangle^{\text{i}^2}}{\langle k\rangle^{\text{i}}} \quad (17)$$

where c_1, c_2, c_3 and c_{k} are constants, $P^{\text{i}} = (-\rho\langle\overline{\mathbf{u}'\mathbf{u}'}\rangle^{\text{i}}:\nabla\bar{\mathbf{u}}_{\text{D}})$ is the production rate of $\langle k\rangle^{\text{i}}$ due to gradients of $\bar{\mathbf{u}}_{\text{D}}$, $G^{\text{i}} = c_{\text{k}}\rho\frac{\phi\langle k\rangle^{\text{i}}|\bar{\mathbf{u}}_{\text{D}}|}{\sqrt{K}}$ is the generation rate of the intrinsic average of k due to the action of the porous matrix and $G^{\text{i}}_{\beta} = \phi\frac{\mu_{\text{t}_\phi}}{\sigma_{\text{t}}}\beta_\phi\mathbf{g}\cdot\nabla\langle\overline{T}\rangle^{\text{i}}$ is the generation rate of $\langle k\rangle^{\text{i}}$ due to the buoyant effects. Here, it is also important to emphasize that mechanical dispersion was not considered in the transport of $\langle k\rangle^{\text{i}}$ and $\langle\,\varepsilon\rangle^{\text{i}}$, as was the case for the mean momentum equation (4). For highly porous and permeable media, for a fluid flowing with a high value of Re_{p}, turbulence interactions are expected to transport momentum and turbulent kinetic energy as a rate faster than that due to dispersion mechanisms.

Further, the constants used in Eqs. (7),(16) and (17) of the macroscopic κ–ε model were the same given by Launder and Spalding [44] for clear medium ($\phi = 1$ and $K\to\infty$). They read,

$$c_\mu = 0,09,\ c_1 = 1,44,\ c_2 = 1,92,\ c_3 = 1,0,$$
$$\sigma_k = 1,0,\ \sigma_\varepsilon = 1,3,\ \sigma_T = 0,9 \quad (18)$$

For a porous medium, these constants may present different values but, as a first approximation, they were taken as equal to those in [44], as suggested by Lee and Howell [9].

Further, standard wall function has been employed for calculating the flow near to the walls, as discussed in [19]. The use of such simpler model is justified due to the final velocity values close to the interface will be a function not only of inertia and viscous effects in full Navier–Stokes equation, but also due to the Darcy and Forchheimer resistance terms. Therefore, eventual errors coming from inaccurate use of more appropriate boundary conditions will have little influence on the final value for velocity close to the wall since drag forces, caused by the porous structure, will play also an important role in determining the final value for the wall velocity. Thus, logarithm wall laws are simple to be incorporated when simulating flow over rigid surfaces and for that they have been modified to include surface roughness and to simulate flows over irregular surfaces at the bottom of rivers [48]. Detailed information on such numerical treatment can be found in [13–16].

5. Numerical method and solution procedure

The numerical method employed for discretizing the governing equations is the control-volume approach with a generalized grid. A hybrid scheme, upwind differencing scheme (UDS) and central differencing scheme (CDS), is used for interpolating the convection fluxes. The well-established SIMPLE algorithm [45] is followed for handling the pressure-velocity coupling. Individual algebraic equation sets were solved by the SIP procedure of [46]. In addition, concentration of nodal points closer to the walls reduces eventual errors due to numerical diffusion which, in turn, are further annihilated due to the hybrid scheme here adopted.

6. Results and discussion

In order to guarantee grid independent solutions, runs were performed in grids up to 110×110 control volumes, using stretched meshes for turbulent flow with $Ra_m = 10^6$. The percent difference of the averaged Nusselt number at the hot wall, compared with results obtained with the 80×80 grid, is 1.15%. Therefore, the 80×80 stretched mesh seems to be refined enough near to the walls to capture the thin boundary layers that appear along the vertical surfaces.

6.1. Laminar model solution

Runs for laminar model solution were performed with an 80×80 control volumes in a stretched grid like shown in Fig. 1(b). The present results were performed with $\phi = 0.8$ and the Prandtl number and the conductivity ratio between the solid and fluid phases are assumed to be a unit. The available literature shows that for the non-Darcy region, [47], the fluid flow and the heat transfer depend on the fluid Rayleigh number, Ra_f and the Darcy number, Da, when other parameters, e.g., (Porosity, Prandtl number, conductivity ratio between the fluid and solid matrix) are fixed.

Thus, herein, porosity, Prandtl number and conductivity ratio were kept fixed. It is also important to emphasize that all runs were performed without the contribution of the thermal dispersion, $\mathbf{K}_{disp}$. However, a few cases considering the effect of thermal dispersion on the Nusselt number were also computed in order to show its influence on the overall heat transport.

Table 1 shows some previous laminar numerical results for Ra_m ranging from 10 to 10^4. Table 2 shows the average Nusselt number for different Darcy numbers for Ra_m ranging from 10 to 10^4. It is clearly seen from the Table 2 that for a fixed Ra_m the lower the permeability, the higher the average Nusselt number at the hot wall. It is evident that different combinations of Ra_f and Da yields different heat transfer results. The increasing of the fluid Rayleigh number increases the natural

Table 1
Some previous laminar numerical results for average Nusselt number for Ra_m ranging from 10 to 10^4

	Ra_m			
	10	10^2	10^3	10^4
Walker and Homsy, [36]	–	3.097	12.96	51.0
Bejan, [37]	–	4.2	15.8	50.8
Beckerman et al., [39]	–	3.113	–	48.9
Gross et al., [40]	–	3.141	13.448	42.583
Manole and Lage, [41]	–	3.118	13.637	48.117
Moya et al., [42]	1.065	2.801	–	–
Baytas and Pop, [43]	1.079	3.16	14.06	48.33

Table 2
Behavior of the average Nusselt number for different values of Da for Ra_m ranging from 10 to 10^4

Da	$\mathbf{K}_{disp}$	Ra_m			
		10	10^2	10^3	10^4
10^{-7}	$\mathbf{K}_{disp}$ given by (11)	1.0907	3.0866	12.9641	41.7693
10^{-7}	$\mathbf{K}_{disp} = 0$	1.0902	3.0831	12.8930	38.6494
10^{-8}	$\mathbf{K}_{disp} = 0$	1.0908	3.0979	13.2751	43.5799
10^{-9}	$\mathbf{K}_{disp} = 0$	1.0910	3.0985	13.3848	46.1659
10^{-10}	$\mathbf{K}_{disp} = 0$	1.0912	3.1016	13.4289	47.2653

convection inside the enclosure. Since the Ra_m is fixed, a higher fluid Rayleigh number is associated with a less permeable media (i.e. lower Darcy number). Its also clearly seen from Table 2 that the Nusselt numbers computed with the thermal dispersion are higher than those computed without it for $Da = 10^{-7}$. It seems evident that this additional mechanism increases heat transfer. Table 2 also shows that for higher values of Ra_m, the effect of the thermal dispersion on the Nusselt number are more pronounced. However, although not shown here, the computational cost due to the inclusion of this mechanism increases significantly. In comparison with results of Table 1, more accurate simulations were obtained for lower permeability media.

The local Nusselt number on the hot wall for the square cavity at $x = 0$ is defined as,

$$Nu = hL/k_{eff} \therefore Nu = \left(\frac{\partial\langle T\rangle^{v}}{\partial x}\right)_{x=0} \frac{L}{T_H - T_C} \tag{19}$$

and the average Nusselt number is given by,

$$\overline{Nu} = \frac{1}{H}\int_0^H Nu\,dy \tag{20}$$

Fig. 2 shows streamlines and isotherms for a laminar model solution in a square cavity filled with porous medium for Ra_m ranging from 10^3 to 10^6. The cavity is heated of the left side and cooled from the opposing side. The other two walls are kept insulated.

For lower Rayleigh number values, $Ra_m \leqslant 10^2$, not shown here, the isotherms are almost parallel to the heated walls, indicating that the most part of heat transfer is by conduction mechanism, while the streamlines are a single vortex with its center in the center of the square cavity.

At $Ra_m = 10^3$, Fig. 2(b), the streamlines are an elliptic flattened vortex. In contrast with the clear cavity case the porous matrix makes the flow be more intense near the heated and cooled walls and damped in the center due to the presence of the porous matrix. Corresponding Isotherms are shown in Fig. 2(a). The enhancing of the natural convection begins to distort the isotherms. The vortex is generated due the horizontal temperature gradient across the section. This gradient, $\delta T/\delta y$, is negative everywhere, giving a clockwise vertical rotation.

Increasing Ra_m to 10^4, Fig. 2(d), the central vortex becomes rectangular and the effect of convection is now more pronounced in the isotherms, as can be seen in Fig. 2(c). The flow pattern comprises a primary cell of relatively high velocity, circulating around the entire cavity. Temperature gradients are stronger near the vertical walls, but decrease in the center.

For higher values of Rayleigh numbers, $Ra_m = 10^5$ and 10^6, the flow moves faster close to heated walls, Fig. 2(f) and (h), and the isotherms tends to stratification, Fig. 2(e) and (g), respectively.

6.2. Turbulent model solution

It is important to emphasize that the main objective of this work is not to simulate the transition mechanism from laminar regime to fully turbulent flow, which involves modeling of complex physical processes and hydrodynamic instabilities. Here, the aim of this work is to establish a Ra_{cr} below which both turbulent and laminar models did not differ substantially as far as predictions of overall Nu are of concern. Therefore, a strategy for determining the range of validity of a laminar flow solution was to simulate the *laminarization* of the flow when the Raleigh number is reduced.

For clear flows, when Ra_f is varied, the literature often refers to laminar and turbulent "branches" of solutions as Ra_f passes a critical value. When a turbulence model is included, the turbulent solution can deviate from the laminar branch for $Ra_f > Ra_{cr}$ and follows its turbulent branch. According to [31], the deviation of the averaged wall-heat transfer between laminar and turbulent fields depends on the turbulence model used.

When the standard κ–ε model is used, the laminar solution is not a solution of the equation system, because it does not satisfy the boundary condition, namely wall function, for the kinetic energy at the first inner grid point close to the wall. Below a critical Ra_f number, the standard κ–ε model gives a turbulent viscosity close to zero everywhere. This reduction of turbulent transfer can be interpreted as an indication of the laminarization process. However, above this critical value, the turbulent viscosity suddenly increases and a turbulent solution is obtained.

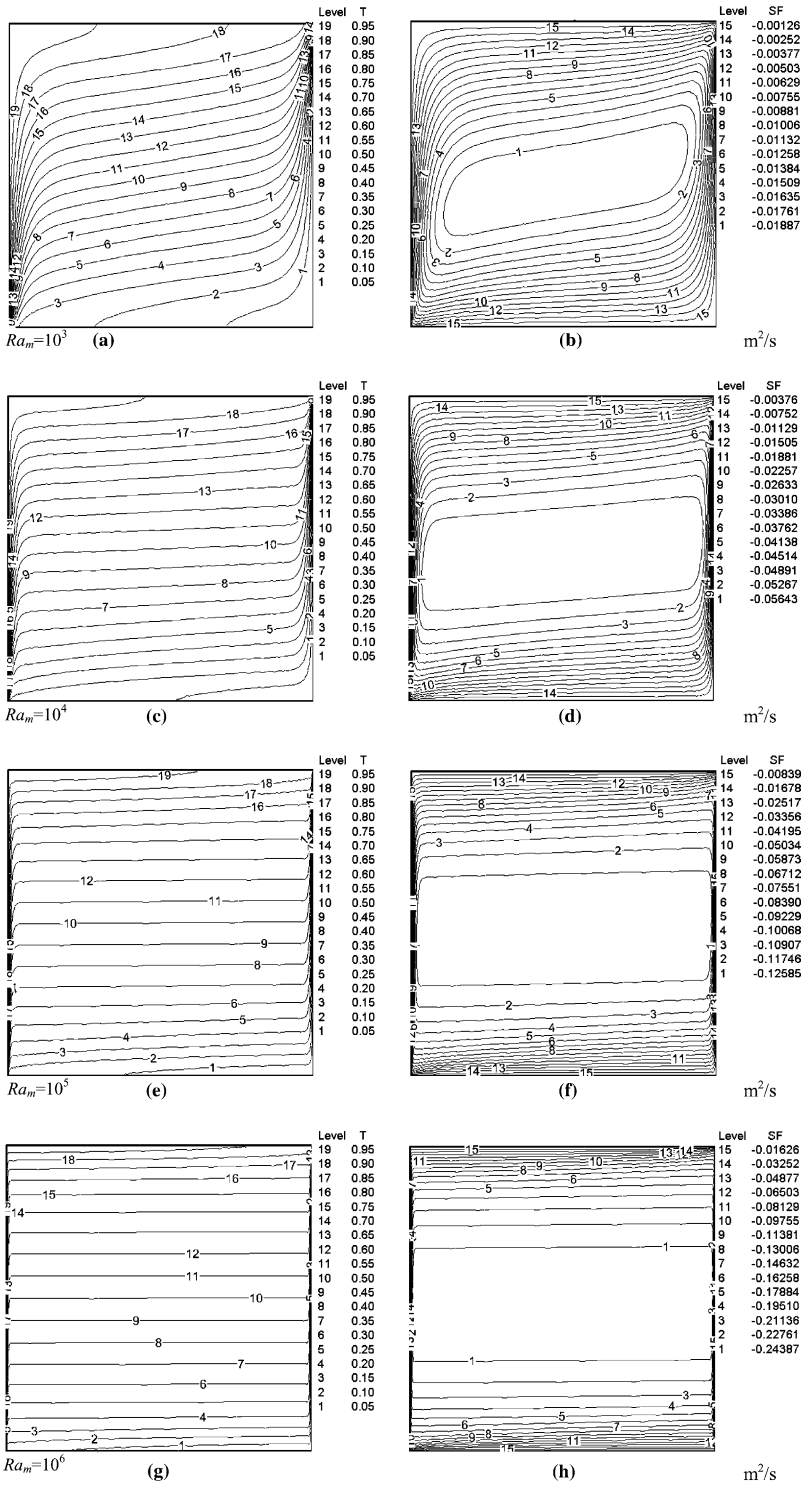

Fig. 2. Isotherms and streamlines for laminar model solution for a square cavity filled with porous material with $\phi = 0.8$, $Da = 10^{-7}$ and $\mathbf{K}_{\text{disp}} = 0$.

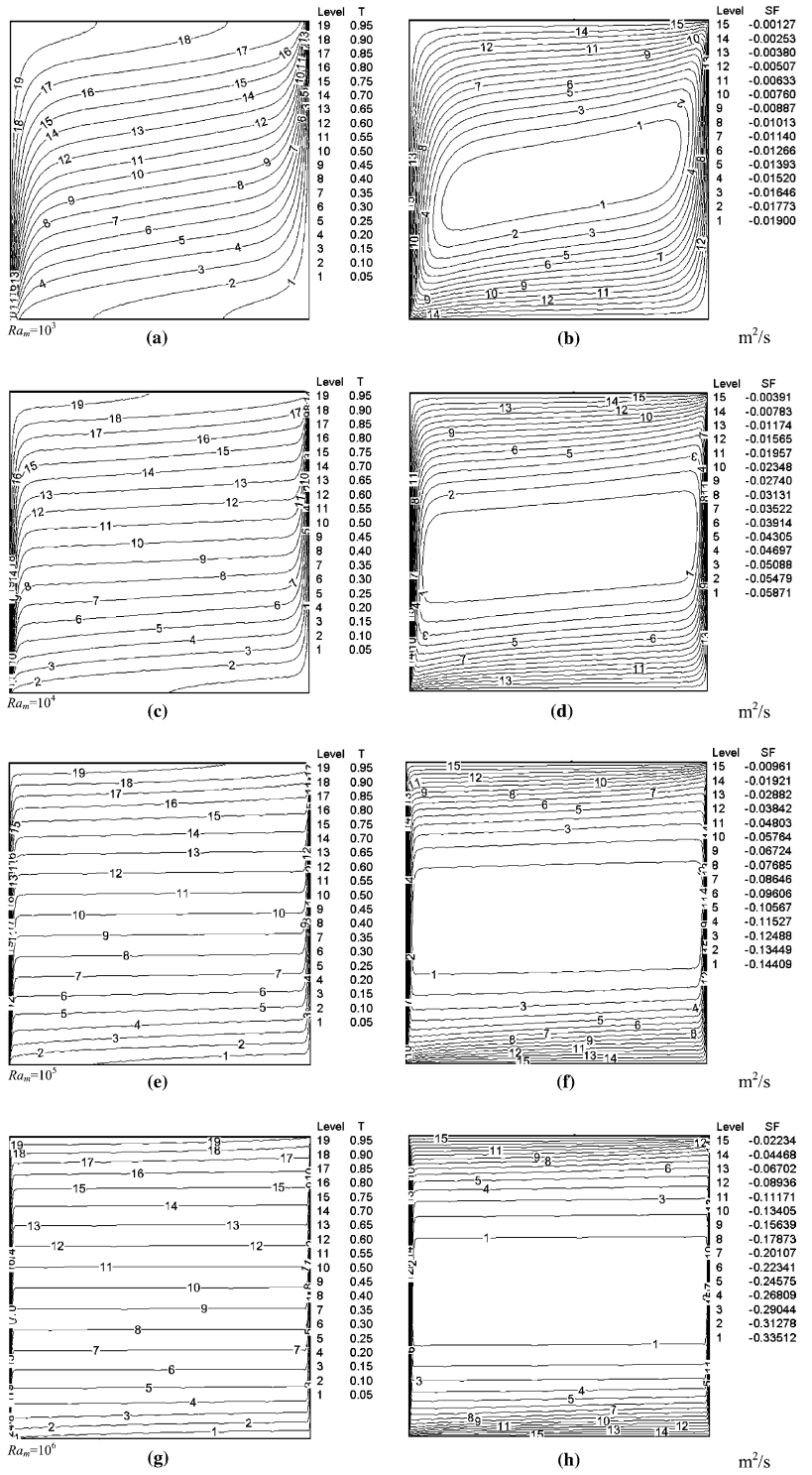

Fig. 3. Isotherms and streamlines for turbulent model solution for a square cavity filled with porous material with $\phi = 0.8$, $Da = 10^{-7}$ and $\mathbf{K}_{\text{disp}} = 0$.

Table 3
Comparison between laminar and turbulent model solutions for the average Nusselt number at the hot wall for $Da = 10^{-7}$ and 10^{-8} and Ra_m ranging from 10 to 10^6

Model solution	Ra_m					
	10	10^2	10^3	10^4	10^5	10^6
$Da = 10^{-7}$ with $\mathbf{K}_{disp}$ given by (11)						
Laminar	1.0907	3.0866	12.9641	41.7693	110.1664	–
Turbulent	1.0910	3.0896	13.0652	43.2809	120.4175	–
$Da = 10^{-7}$ with $\mathbf{K}_{disp} = 0$						
Laminar	1.0902	3.0831	12.8930	38.6494	87.3268	169.9404
Turbulent	1.0907	3.0860	12.9956	40.3077	100.6035	235.5515
$Da = 10^{-8}$ with $\mathbf{K}_{disp} = 0$						
Laminar	1.0908	3.0979	13.2751	43.5799	109.1877	222.5915
Turbulent	1.0910	3.1006	13.3525	44.7605	119.1966	277.0930

With this ideas in mind, this part of the work tries to find for flow in porous media, as done in the literature for the clear fluid case, like in [31] and [33], a critical Rayleigh, Ra_{cr}, for which simulations with the turbulence model deviates from those considering laminar flow. In order to achieve this goal, the turbulence model is first "switched off" and the laminar branch of the solution is found when increasing the Rayleigh number, Ra_m. Subsequently, the turbulence model is included so that the solution merges to the laminar branch for a reducing Ra_m and for $Ra_m < Ra_{cr}$. This convergence of results as Ra_m decreases can be seen to characterize the so-called *laminarization* phenomenon.

Calculations for turbulent model solution were performed with the same grid used for the laminar model solution and the parameters (porosity, Prandtl number and conductivity ratio between the fluid and the solid matrix) are fixed.

Fig. 3 shows the isotherms and streamlines for turbulent model solution for Ra_m ranging from 10^3 to 10^6. For $Ra_m \leqslant 10^2$, not shown here, the solution with the turbulence model gives nearly the same values as those obtained with laminar flow computations. Even for Ra_m up to 10^6 the flow patterns resembles those from the laminar model solution, but the values of the streamlines and the average Nusselt numbers at the hot wall are significantly increased.

Table 3 shows the average Nusselt number at the hot wall for the two types of regime, namely laminar and turbulent for two distinct Darcy numbers. Table 3 shows that the turbulent solution deviates from the laminar one for Ra_m greater than around 10^4. Consequently, the calculations herein suggest that a critical value for Rayleigh is of the order of 10^4 and from that value on simulations considering a turbulence model are higher than their laminar counterpart.

Fig. 4 shows the behavior of the average Nusselt number versus the Rayleigh number for the two models here considered, namely the laminar and the turbulence

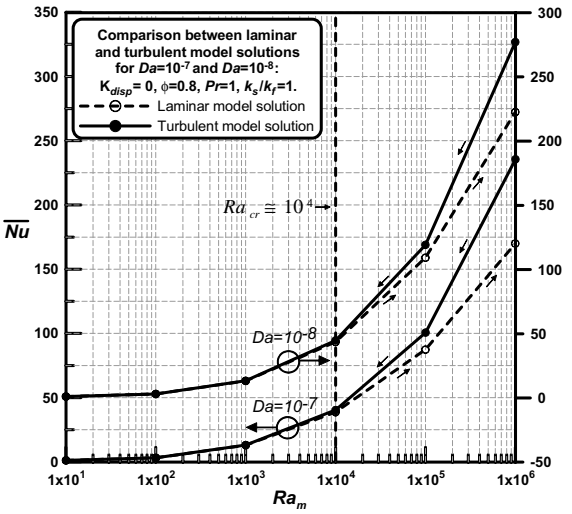

Fig. 4. Comparison between the laminar and turbulent model solutions with the averaged Nusselt number at the hot wall.

models for $Da = 10^{-7}$ and $Da = 10^{-8}$ illustrating the two regions mentioned above. It is clearly seen from Fig. 4 that Ra_{cr} is not affected due to small variations on the Darcy number.

In the first region for $Ra_m < Ra_{cr} \sim 10^4$, both laminar and turbulent flow simulations give nearly the same results. After this point, Nusselt numbers calculated with a full turbulence model give higher values for $\overline{Nu}$.

7. Conclusion

Computations for laminar and turbulent flows with the macroscopic κ–ε model with a wall function for natural convection in a square cavity totally filled with porous material were performed. The cavity was heated from the left and cooled from the opposing side. The numerical values yielded generally satisfactory agree-

ment with similar data available in the literature. This agreement was also found when comparing average Nusselt numbers along the hot wall.

In general, when fluid and medium properties (Prandtl number, porosity and conductivity ratio between the fluid and the solid matrix) are kept fixed and Ra_m is constant, the lower the Darcy number (or media permeability), the higher the average Nusselt number at the hot wall. The increasing of the fluid Rayleigh number increases the natural convection inside the enclosure. Since the Ra_m is fixed, a higher fluid Rayleigh number is associated with a less permeable media (i.e. lower Darcy number). In the end, for Ra_m values greater than around 10^4, both laminar and turbulent flow solutions deviate from each other, indicating that such critical value for Ra_m was reached. Accordingly, in order to observe that, the turbulence model was first switched off and the laminar branch of the solution was found when increasing the Rayleigh number, Ra_m. Subsequently, the turbulence model was included so that the solution merged to the laminar branch for $Ra_m < Ra_{cr}$. This convergence of results as Ra_m decreases can be seen as an estimate of the so-called *laminarization* phenomenon.

Ultimately, the inclusion of thermal dispersion increases the Nusselt number on the hot wall by a fair amount for higher Ra_m, since it represents an additional mechanism of mixing. However, the inclusion of this effect also significantly reduces convergence rates and associated computational cost. Further, Ra_{cr} is not affected due to the inclusion of the thermal dispersion mechanism, $\mathbf{K}_{disp}$, or due to small variations on the Darcy number.

Acknowledgments

The authors are thankful to CNPq and FAPESP, Brazil, for their invaluable financial support during the course of this research.

References

[1] C.T. Hsu, P. Cheng, Thermal dispersion in a porous medium, Int. J. Heat Mass Transfer 33 (1990) 1587–1597.
[2] J. Bear, Dynamics of Fluids in Porous Media, American Elsevier Pub. Co., New York, 1972.
[3] S. Whitaker, Equations of motion in porous media, Chem. Eng. Sci. 21 (1966) 291–300.
[4] S. Whitaker, Diffusion and dispersion in porous media, J. Am. Inst. Chem. Eng. 13 (3) (1967) 420–427.
[5] T. Masuoka, Y. Takatsu, Turbulence model for flow through porous media, Int. J. Heat Mass Transfer 39 (13) (1996) 2803–2809.
[6] F. Kuwahara, A. Nakayama, H. Koyama, A numerical study of thermal dispersion in porous media, J. Heat Transfer 118 (1996) 756–761.
[7] F. Kuwahara, A. Nakayama, Numerical modeling of non-Darcy convective flow in a porous medium, Heat Transfer 1998Proc. 11th Int. Heat Transf. Conf., Kyongyu, Korea, 4, Taylor & Francis, Washington, DC, 1998, pp. 411–416.
[8] A. Nakayama, F. Kuwahara, A macroscopic turbulence model for flow in a porous medium, J. Fluids Eng. 121 (1999) 427–433.
[9] K. Lee, J.R. Howell, Forced convective and radiative transfer within a highly porous layer exposed to a turbulent external flow fieldProceedings of the 1987 ASME-JSME Thermal Engineering Joint Conf., Honolulu, Hawaii, 2, ASME, New York, N.Y, 1987, pp. 377–386.
[10] B.V. Antohe, J.L. Lage, A general two-equation macroscopic turbulence model for incompressible flow in porous media, Int. J. Heat Mass Transfer 40 (13) (1997) 3013–3024.
[11] D. Getachewa, W.J. Minkowycz, J.L. Lage, Int. J. Heat Mass Transfer 43 (2000) 2909–2915.
[12] M.H.J. Pedras, M.J.S. de Lemos, On the definition of turbulent kinetic energy for flow in porous media, Int. Commun. Heat Mass Transfer 27 (2) (2000) 211–220.
[13] M.H.J. Pedras, M.J.S. de Lemos, Macroscopic turbulence modeling for incompressible flow through undeformable porous media, Int. J. Heat Mass Transfer 44 (6) (2001) 1081–1093.
[14] M.H.J. Pedras, M.J.S. de Lemos, Simulation of turbulent flow in porous media using a spatially periodic array and a low-re two-equation closure, Numer. Heat Transfer, Part A 39 (1) (2001) 35–39.
[15] M.H.J. Pedras, M.J.S. de Lemos, On the mathematical description and simulation of turbulent flow in a porous medium formed by an array of elliptic rods, J. Fluids Eng. 123 (4) (2001) 941–947.
[16] M.H.J. Pedras, M.J.S. de Lemos, Computation of turbulent flow in porous media using a low reynolds κ–ε model and a infinite array o transversally-displaced elliptic rods, Numer. Heat Transfer, Part A 43 (6) (2003) 585.
[17] F.D. Rocamora Jr, M.J.S. de Lemos, Analysis of convective heat transfer of turbulent flow in saturated porous media, Int. Commun. Heat Mass Transfer 27 (6) (2000) 825–834.
[18] M.J.S. de Lemos, F.D. Rocamora, Turbulent transport modeling for heated flow in rigid porous media, in: Proc. of the Twelfth Int. Heat Transfer Conf., 2002, pp. 791–795.
[19] R.A. Silva, M.J.S. de Lemos, Turbulent flow in a channel occupied by a porous layer considering the stress jump at the interface, Int. J. Heat Mass Transfer 46 (2003) 5113–5121.
[20] R.A. Silva, M.J.S. de Lemos, Numerical analysis of the stress jump interface condition for laminar flow over a porous layer, Numer. Heat Transfer, Part A 43 (6) (2003) 603–617.
[21] M.J.S. de Lemos, E.J. Braga, Modeling of turbulent natural convection in porous media, Int. Commun. Heat Mass Transfer 30 (5) (2003) 615–624.
[22] M.J.S. de Lemos, M.S. Mesquita, Turbulent mass transport in saturated rigid porous media, Int. Commun. Heat Mass Transfer 30 (1) (2003) 105–113.
[23] M.J.S. de Lemos, L.A. Tofaneli, Modeling of double-diffusive turbulent natural convection in porous media, Int. J. Heat Mass Transfer 47 (2004) 4233–4241.

[24] M.J.S. de Lemos, M.H.J. Pedras, Recent mathematical models for turbulent flow for saturated rigid porous media, J. Fluids Eng. 123 (4) (2001) 935–940.
[25] H. Bérnard, Les tourbillons cellulaires dans une nappe liquide transportant de la chaleur par convection em régime permanent, Ann. Chim. Phys. 23 (1901) 62–144.
[26] Lord J.W. Strutt Rayleigh, On convection currents in a horizontal layer of fluid when the higher temperature is on the underside, Philos. Mag. 32 (ser. 6) (1926) 833–844.
[27] I.P. Jones, A comparison problem for numerical methods in fluid dynamics: the double-glazing problem, in: R.W. Lewis, K. Morgan (Eds.), Numerical Methods in Thermal Problems, Pineridge Press, Swansea, U.K, 1979, pp. 338–348.
[28] G. de Vahl Davis, Natural convection in a square cavity: a benchmark numerical solution, Int. J. Num. Methods Fluids 3 (1983) 249–264.
[29] N.C. Markatos, K.A. Pericleous, Laminar and turbulent natural convection in an enclosed cavity, Int. J. Heat Mass Transfer 27 (1984) 755–772.
[30] H. Ozoe, A. Mouri, M. Ohmuro, S.W. Churchill, N. Lior, Numerical calculations of laminar and turbulent natural convection in water in rectangular channels heated and cooled isothermally on the opposing vertical walls, Int. J. Heat Mass Transfer 28 (1985) 125–138.
[31] R.A.W.M. Henkes, F.F. Van Der Vlugt, C.J. Hoogendoorn, Natural-convection flow in a square cavity calculated with low-Reynolds-number turbulence models, Int. J. Heat Mass transfer 34 (2) (1991) 377–388.
[32] T. Fusegi, J.M. Hyun, K. Kuwahara, Three-dimensional simulations of natural convection in a sidewall-heated cube, Int. J. Numer. Methods. Fluids 3 (1991) 857–867.
[33] G. Barakos, E. Mitsoulis, D. Assimacopoulos, Natural convection flow in a square cavity revited: laminar and turbulent models with wall function, Int. J. Numer. Methods Fluids 18 (1994) 695–719.
[34] D.A. Nield, A. Bejan, Convection in Porous Media, Springer, New York, 1992.
[35] D.B. Ingham, I. Pop, Transport Phenomena in Porous Media, Elsevier, Amsterdam, 1998.
[36] K.L. Walker, G.M. Homsy, Convection in porous cavity, J. Fluid Mech. 87 (1978) 49–474.
[37] A. Bejan, On the boundary layer regime in a vertical enclosure filled with a porous medium, Lett. Heat Mass transfer 6 (1979) 93–102.
[38] V. Prasad, F.A. Kulacki, Convective heat transfer in a rectangular porous cavity-effect of aspect ratio on flow structure and heat transfer, J. Heat Transfer 106 (1984) 158–165.
[39] C. Beckermann, R. Viskanta, S. Ramadhyani, A numerical study of non-Darcian natural convection in a vertical enclosure filled with a porous medium, Numer. Heat Transfer 10 (1986) 557–570.
[40] R.J. Gross, M.R. Bear, C.E. Hickox, The application of flux-corrected transport (FCT) to high rayleigh number natural convection in a porous medium, in: Proc, 8th Int. Heat transfer Conf., San Francisco, CA, 1986.
[41] D.M. Manole, J.L. Lage, Numerical benchmark results for natural convection in a porous medium cavity, HTD-Vol 216, Heat and mass Transfer in Porous Media, ASME Conference, 1992, pp. 55–60.
[42] S.L. Moya, E. Ramos, M. Sen, Numerical study of natural convection in a tilted rectangular porous material, Int. J. Heat Mass Transfer 30 (1987) 741–756.
[43] A.C. Baytas, I. Pop, Free convection in oblique enclosures filled with a porous medium, Int. J. Heat Mass Transfer 42 (1999) 1047–1057.
[44] B.E. Launder, D.B. Spalding, The numerical computation of turbulent flows, Comput. Methods Appl. Mech. Eng. 3 (1974) 269–289.
[45] S.V. Patankar, D.B. Spalding, A calculation procedure for heat, mass and momentum transfer in three dimensional parabolic flows, Int. J. Heat Mass Transfer 15 (1972) 1787.
[46] H.L. Stone, Iterative solution of implicit approximations of multi-dimensional partial differential equations, SIAM J. Numer. Anal. 5 (1968) 530–558.
[47] A.A. Merrikh, A.A. Mohamad, Non-Darcy effects in buoyancy driven flows in an enclosures filled with vertically layered porous media, Int. J. Heat Mass Transfer 45 (2002) 4305–4313.
[48] S.N. Lane, R.J. Hardy, Porous rivers: a new way of conceptualizing and modeling river and floodplain flows? in: D. Ingham, I. Pop (Eds.), Transport Phenomena in Porous Media II, first ed., Pergamon Press, 2002, pp. 425–449 (Chapter 16).